Suppression of Trapped Energetic Ions Driven Resistive Interchange Modes with Electron Cyclotron Heating in a Helical Plasma

X. D. Du,[1,*] K. Toi,[1] S. Ohdachi,[1,2] K. Y. Watanabe,[1,2] H. Takahashi,[1,2] Y. Yoshimura,[1] M. Osakabe,[1,2] R. Seki,[1,2]
T. Nicolas,[1] H. Tsuchiya,[1] K. Nagaoka,[1] K. Ogawa,[1,2] K. Tanaka,[1] M. Isobe,[1,2] M. Yokoyama,[1,2]
M. Yoshinuma,[1,2] S. Kubo,[1] S. Sakakibara,[1,2] T. Bando,[2] T. Ido,[1] T. Ozaki,[1] Y. Suzuki,[1,2]
Y. Takemura[1,2] and LHD Experiment Group[1]

[1]*National Institute for Fusion Science, 509-5292 Toki, Japan*
[2]*Department of Fusion Science, The Graduate University for Advanced Studies, 509-5292 Toki, Japan*
(Received 8 August 2016; revised manuscript received 25 January 2017; published 20 March 2017)

The resistive interchange mode destabilized by the resonant interaction with the trapped energetic ions is fully suppressed when the injected power of electron cyclotron heating exceeds a certain threshold. It is shown for the first time that the complete stabilization of the energetic-particle-driven mode without relaxing the energetic particle (EP) pressure gradient is possible by reducing the radial width of the eigenmodes δ_w, especially when δ_w narrows to a small enough value relative to the finite orbit width of EP.

One of the key issues to sustain the burning plasma in future fusion reactors, i.e., tokamak and stellarator or helical devices, is to reduce an excessive loss of energetic particles (EPs), such as α particles. The confinement of the EP often largely deteriorates when resonant interactions between the EP and magnetohydrodynamics (MHD) waves occur [1–4]. In recent years, much attention has been paid to the development of reliable control techniques for mitigation or even suppression of dangerous EP-driven MHD instabilities. For example, it is well documented that the localized deposition of electron cyclotron heating (ECH) power near the minimum of the magnetic safety factor $q_{\min}$ sometimes suppresses the reversed-shear Alfvén eigenmodes in DIII-D tokamak [5,6] through finite pressure effects [7]. It is also reported that a temporary transition of bursting Alfvén modes into a saturated continuous mode with reduced magnitude is observed after the application of static 3D magnetic field perturbations (MP) in National Spherical Torus Experiment [8]. It is concluded that the reduction of the fast ion drive by the MP-induced losses of the resonant EPs is responsible for the observed mitigation, so called "phase-space engineering" [9]. In the large helical device (LHD), the resistive interchange mode (RIC), which is destabilized in the unfavorable average curvature region by the plasma pressure gradient, can abruptly evolve into a dangerous bursting mode with a large amplitude and rapid frequency chirping when a large population of the trapped EPs is produced by the intense injection of hydrogen neutral beams nearly perpendicular to the magnetic axis (PERP-NBI). This bursting mode is identified as the helically trapped EP-driven resistive interchange mode or "EIC" in previous work [10,11]. The EIC resonates with the precession motion of the helically trapped EPs and induces significant losses. This Letter reports the experimental efforts on the control of the EIC with ECH. It is found that when the

on-axis electron cyclotron wave (ECH/ECW) power exceeds a certain threshold, the EIC locating in the plasma peripheral region can be fully suppressed.

A bursting behavior of magnetic fluctuations occurs in the low frequency range of $f < 10$ kHz, when PERP-NBI is applied to a low-density plasma with a magnetic field strength of $B_t = -2.85$ T at the magnetic axis, as shown in Fig. 1(a1). Each burst grows from a weakly destabilized oscillation having a constant frequency of $\sim$4 kHz, suddenly reaches the large amplitude and has the initial frequency of $\sim$8 kHz, and then rapidly chirps down.
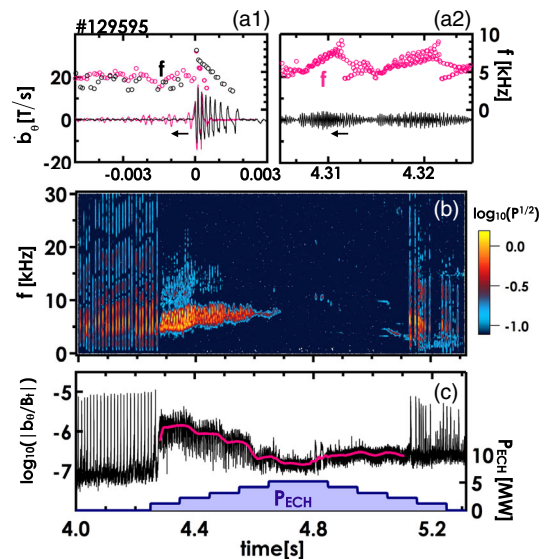
FIG. 1. Time evolutions of the zoomed waveforms of the magnetic fluctuations and the frequencies for the bursty EICs (a1) and continuous oscillatory mode (a2), the power spectra of the magnetic fluctuation (b) and the normalized integrated magnetic fluctuation with the varied ECH/ECW power (c).

The weakly destabilized oscillation is considered as the RIC since the edge region of the LHD plasma is stable for ideal interchange modes due to appreciable magnetic shear effect, and the experimentally obtained radial plasma displacement is recognized to be an even function and highly localized at the $\iota = 1$ surface (ι: rotational transform), i.e., $r/a \sim 0.88$ (a: averaged minor radius). The mode exhibiting a bursting nature of the amplitude and rapid frequency chirping was identified as the EIC [10,11]. In order to control the EIC, the ECW are launched from three 77 GHz and two 154 GHz gyrotrons, each generating 1 MW port-through power to plasma. Here, the 77 GHz (154 GHz) is the fundamental (second harmonic) resonance frequency for magnetic field strength B_t of 2.75 T. In this experiment, the ECW power using a staircase function up to 5 MW is employed, shown in Fig. 1(c). About 92% of the total power is absorbed in the plasma core of $r/a < 0.5$, and no power is absorbed in the plasma peripheral region of $r/a > 0.8$, estimated by the TRAVIS code [12]. Note that from $t = 4.35$ s the ECW power is mixed with normal and oblique injections towards the plasma center, but all power contributes only to electron heating near $\iota = 1$ surface. Hereafter, "ECW injection" is expressed simply as "ECH".

A significant change of the EIC behavior is observed ~ 40 ms after the switch on of the 1.2 MW ECH at $t = 4.25$ s. The major change is that the intermittent bursty EICs with large amplitudes are suppressed and just after, a continuous oscillation mode is excited with appreciable amplitude, as shown in Fig. 1(a2). The frequency gradually sweeps up from ~ 5 kHz to ~ 8 kHz in ~ 8 ms and later back to 5 kHz in ~ 2 ms. The change is also discernible when the power increases with a 1 MW step. That is, the oscillatory mode further reduces the amplitude and the range of the frequency upsweep in each step, as seen from Figs. 1(b) and 1(c). It should be noted that it takes about ~ 40 ms with a good reproducibility for the magnetic fluctuation to decrease after the increase in the power. The time is comparable with that needed for electrons to reach the new thermal equilibrium after increasing the heating power, suggested by electron cyclotron emission (ECE). The oscillatory mode disappears when the power reaches 5 MW. The recurrence of the bursty EIC does not take place until the power decreases back to 2 MW at $t \sim 5.13$ s. The sequential response of the mode behaviors on ramping up (down) the power by switching on (off) the gyrotrons with different frequencies, but with the same heating efficiencies of $\sim 100\%$, suggests that the total injected power contributing to intense electron heating is the key to the suppression process, regardless of the fundamental or second harmonic heating scenario. In a dedicated experimental campaign of ~ 20 shots with an on-axis ECH power of ~ 5 MW without the multistep power scan, the complete suppression of the bursty EICs having a wide range of amplitude are achieved.
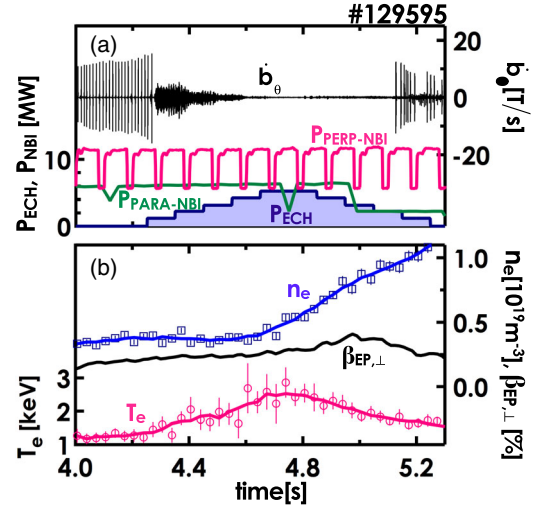
FIG. 2. Time evolutions of magnetic fluctuation $\dot{b}_\theta$, the port-through power of the PERP-NBI, PARA-NBI, and ECH (a) and the measured n_e, T_e at the mode rational surface together with the volume-averaged beta of helically trapped EPs (b).

It is reported that the bursty EIC induces the sudden plasma potential drop and the energetic charge-exchanged neutral particle flux increases by EP transport to the neutral-rich edge region [11]. Importantly, such signatures of the appreciable EP losses are not observed during the oscillatory mode as having slow frequency chirping, which would indicate weak mode-EP interaction. Moreover, the time derivative of the diamagnetic signal also does not indicate the EP losses as observed in bursty EIC [11].

Figure 2(b) shows that the on-axis ECH strikingly raises electron temperature T_e even at $\iota = 1$ surface near the edge by a factor of three. Meanwhile, the electron density n_e is almost constant from 4.25 s to 4.6 s, and later begins to rise continuously, of which temporal evolution of n_e can be explained by competition between neutral fueling by PERP-NBI and density pumpout by ECH. Therefore, before raising the n_e, the dynamical friction of beam ions by the background electrons is reduced without altering the friction by background ions, leading to a slight increase of total EP content. Later, the increase of n_e will exponentially decrease the shine-through rate η_{ST} of the neutral beam as $\eta_{ST} = \exp(-\sigma_{eff} n_e L)$, where σ_{eff} is the effective cross section for ionization by bulk plasma and L is the neutral beam flight path [13]. It is reflected on the increased volume-averaged beam beta of helically trapped EPs, $\beta_{EP,\perp}$, shown in Fig. 2(b). The trapped energetic ions' density profiles, calculated from a beam deposition code "FIT3D" [14] using the measured profiles of T_e and n_e, support the increase of $\beta_{EP,\perp}$, as shown in Fig. 3. Here, $\beta_{EP,\perp}$ is estimated as $\beta_{EP,\perp} = \beta_d - \beta_b$, where β_d is the diamagnetic beta obtained by a diamagnetic loop, and β_b is the bulk plasma beta derived from Thomson scattering diagnostics and charge exchange spectroscopy. The decrease of $\beta_{EP,\perp}$ from $t \sim 5.0$ s is due to the step down of one neutral
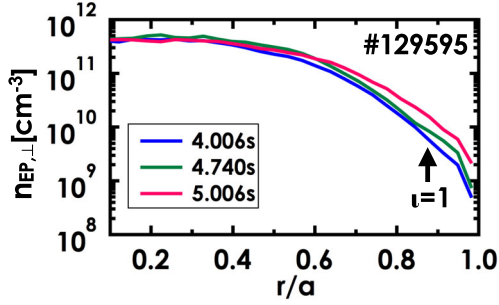
FIG. 3.   The deposited density profile from PERP-NBI of 1 MW at $t = 4.006$ s, $t = 4.74$ s, and $t = 5.006$ s, estimated by FIT3D code, respectively.

hydrogen beam line nearly parallel to the magnetic axis (PARA-NBI), shown in Fig. 2(a). The fact that the EICs are suppressed, even when trapped EP contents around the mode rational surface are clearly increasing, indicates that the threshold of the EIC destabilization is raised by superimposing the ECH to NBI-heated plasma.

One common fact of the EIC without the ECH is that both the expansion of the radial mode width and the increase in amplitude of the RIC just before the onset of the EIC are often observed, accompanied by an appreciable increase of the magnetic fluctuation, as seen from Fig. 4(a). Here, only the electron temperature fluctuation δT_e associated with the RIC is represented in order to emphasize the behavior. Figure 4(b) summarizes the radial widths of the RICs, which are followed by the excitation of EICs for 19 bursts (triangles) and which are not (dots), over magnetic fluctuation in a steady-state plasma with the constantly injected power of PERP-NBI. The mode width δ_w is crudely estimated from a Gaussian model of $\delta T_e = A_0 \exp[-(r - r_m)^2/\delta_w^2]$, where A_0 is the maximum amplitude of $|\delta T_e|$ and r_m is the mode center on the assumption that δT_e is a function of the magnetic flux surface. This figure suggests that the poloidal magnetic fluctuation b_θ, measured by magnetic probe, is nearly proportional to the estimated mode width δ_w. For small amplitude RIC, the magnitude $|(b_\theta/B_t)_{r=r_p>a}|$ at the probe position will be proportional to the value $|(\partial \xi_r/\partial r)_{r=a}|$ at plasma boundary, where radial plasma displacement ξ_r is assumed to be a Gaussian shape, the same as δT_e shown above. The $|(\partial \xi_r/\partial r)_{r=a}|$ increases quasilinearly to δ_w in the parameter ranges shown in Fig. 4(b), i.e., $\delta_w/a < 0.08$ and $(a - r_s)/a \sim 0.125$. More importantly, a certain threshold of δ_w of the RIC exists for the EIC destabilization.

On the other hand, the width of the RIC is found to shrink when the ECH is applied. In Fig. 5(a), the radial profiles of the coherence $\gamma^2_{\delta T_e}$ between the magnetic fluctuation and δT_e, induced by the RIC without ECH and with the ECH of 5 MW, are compared, as well as the phase difference. Note that the $\gamma^2_{\delta T_e}$ profile is thought to be similar to the radial mode structure of the RIC. In this shot, EICs are stabilized by the injection of the ECH power of
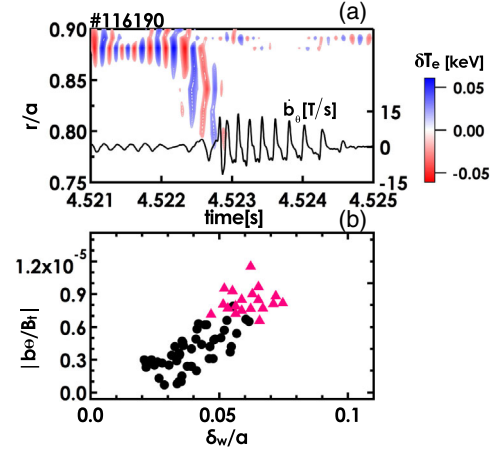
FIG. 4.   Time evolutions of electron temperature fluctuation profiles for $|\delta T_e| \geq 0.02$ keV associated with the RIC (a) and the normalized magnetic fluctuations as the function of the radial width of the RICs, which are followed by the EICs (triangles) and which are not (dots) (b).

5 MW without multistep power scan. The reduction of $\gamma^2_{\delta T_e}$ width by $\sim$50%, preserving the typical interchange-type phase difference, is recognized during the ECH of 5 MW. In the shot No. 129595 with the power scan, the mode structure of the oscillatory mode with the slow frequency upsweep is quite similar to that of the RIC, and the width during the ECH of $\sim$1.2 MW is slightly narrower than that of the RIC before the ECH injection. The continuous shrinkage of oscillatory mode width is observed while increasing the power from $\sim$1.2 MW to $\sim$2.2 MW, shown in Fig. 5(b). The reason why the width during the ECH of $\sim$1.2 MW only shrinks moderately compared with that without the ECH is possibly because the width of the oscillatory mode is expanded by the increased content of trapped EPs at the mode rational surface after suppressing the bursty EIC. These observations indicate that the width of the eigenmodes, i.e., RIC, and the oscillatory mode with frequency upsweep both can be tailored by the ECH.
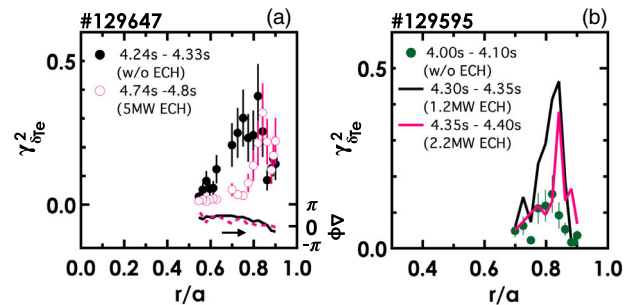
FIG. 5.   (a) Radial profiles of the coherences $\gamma^2_{\delta T_e}$ and phase differences between the magnetic fluctuation and δT_e, induced by the RIC without the ECH and with the ECH of 5 MW in shot 129647. (b) Radial profiles of the $\gamma^2_{\delta T_e}$ induced by the RIC without the ECH and with the ECH of 1.2 MW and 2.2 MW in shot 129595.
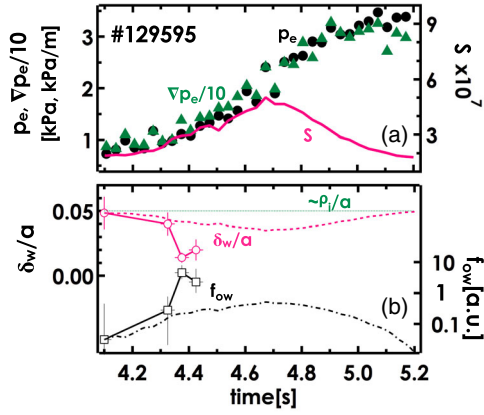
FIG. 6.   Time evolutions of p_e (dots), ∇p_e (triangles), and the estimated S at $\iota = 1$ surface (a) and the δ_w of the RIC and oscillatory mode derived from the $\gamma_{\delta T_e}^2$ profiles (circles) and inferred from the measured plasma parameter change (dashed line), and the varied thresholds for the EIC excitation f_{ow} (squares and dash-dotted line), correspondingly (b).

According to the linear theory, ECH can indeed modify the δ_w through the modification of the background plasma. Discussions on the linear eigenfunction of the RIC may hint at the ECH effects on the observed nonlinear saturated RIC with low amplitude. The parameter dependence of the radial width of the resistive interchange linear eigenfunction in a low β plasma is expressed as [15]

$$\delta_w \propto \left(\frac{q^2}{S\hat{s}^2}\right)^{1/3}\left(\frac{\beta\kappa_n}{L_p}\right)^{1/6}, \qquad (1)$$

where q is the safety factor, S is the local lundquist number, $\hat{s}$ is the magnetic shear parameter, β is the equilibrium pressure normalized by the magnetic pressure, L_p is the scale length of the pressure gradient, and κ_n is the averaged magnetic curvature. The applied ECH brings about the large increase in S by raising local T_e, as shown in Fig. 6(a). This contributes to the reduction of δ_w. Competitively, the increased electron pressure p_e tends towards the expansion of δ_w with much weaker dependence. The L_p, i.e., $L_p^{-1} = \nabla p_e/p_e$, is not noticeably altered. The δ_w, shown with the dashed curve in Fig. 6(b), is roughly estimated from the relation of $\delta_w \propto S^{-1/3}\beta^{1/6}L_p^{-1/6}$, using the measured data obtained before the ECH injection as the reference. It is found that the reduction of the δ_w only due to the ECH-modified T_e and p_e can reach ~20% at maximum. The rapid decrease of δ_w/a, shown with circles in Fig. 6(b), may be assisted with certain secondary effects of ECH. As seen from Fig. 5, the mode peak is shifted outward at the shrinking stage and it is thought to be due to enhanced Shafranov shift caused by a peaked pressure profile by on-axis ECH. This leads to the enhancement of the magnetic shear $\hat{s}$ and would reduce the width more effectively, as seen from Eq. (1). Moreover, it is speculated that the RIC width expansion due to toroidal effects may be

effectively reduced due to the decoupling during gradual shrinkage by increasing S and $\hat{s}$.

It is well known that the growth rate of EP-driven high-n toroidicity-induced Alfvén eigenmodes (TAE) strongly depends on the mode number due to finite orbit width effect in tokamak as $\gamma \propto m^{-2}$ [16–18], as well as in stellarator as $\gamma \propto m^{-1}$ [19]. It is also reported that the growth rate of TAE sharply drops when the orbit widths exceed the radial mode width in stellarator [20]. Likewise, the dispersion relation of the trapped EP-driven resistive interchange-ballooning mode shows that the threshold for the EIC excitation can be altered by the change of radial eigenmode width by a factor of

$$f_{ow} \sim (\rho_i/\delta_w)\ln(\rho_i/\delta_w), \qquad (2)$$

where ρ_i is the orbit width of EPs [21]. In our experiment, finite orbit width, i.e., deviation from the magnetic surface, is estimated to be ~5% of the normalized minor radius by a Lorentz orbit simulation code [22]. The values are, in fact, of the same order of magnitude as the observed δ_w, i.e., $\delta_w \sim \rho_i$, as shown in Fig. 5. Therefore, as seen from Eq. (2), the modification on the δ_w is expected to effectively change the threshold of EIC excitation. For instance, if using $\rho_i/a = 5\%$, the reduction of δ_w/a from ~4.5% to ~2%, observed in the experiment, will lead to the increase of the threshold by a factor of ~20, shown in Fig. 6(b). The reduction of δ_w, only due to increase of S by intense electron heating by using ECH power of 5 MW, will give a rise of the threshold by a factor of ~3. Thus, ECH is considered to be a very powerful tool to control the EIC mode and suppress the losses of trapped energetic ions.

Alternative explanation that the suppression of the EIC is due to the increased damping through the modified perpendicular thermal conductivity is considered to be implausible, according to the simulation results [23,24]. The possibility that the stability of EIC is altered by the presence of a large amount of fast electrons by ECW is also excluded [25] because the mode locates far away from the localized deposition region at the plasma core.

The common finite orbit width stabilization effect on EP-driven ideal or resistive MHD modes suggests that the EP contributes to the mode drive through the entire eigenmode width that consists of both the outer ideal region and the inner resistive layer. Contrary to the modes determined by drive in the ideal region, like internal kink mode or AE modes, the RIC strongly depends on the parameter within the resistive layer [26]. In low β plasmas with finite magnetic shear, the resistive layer width of the RIC is almost the same as the entire mode width. In such a condition, EIC would be destabilized through dominant interactions between EPs and the resistive layer [21]. However, as seen from Fig. 5, the observed mode widths are much larger than the resistive layer width without ECH and with low power ECH and are slightly larger

($\sim$30% to 50%) in high power phases. The mode width of RIC, excited in the LHD plasmas without high power ECH, is dominated by the ideal region as similar to tearing mode and ideal modes such as AEs and kink modes. That is, if the mode width of AEs, tearing mode, and kink modes will be reduced down to a much smaller size for the EP orbits, using various techniques such as ECH or local current drive by ECWs, the impacts of the EP-driven modes on plasma performance would be controlled through a similar mechanism that is observed for RIC in LHD plasmas.

————

[*]Corresponding author.
duxiaodi@fusion.gat.com
Present Address: Department of Physics & Astronomy, University of California-Irvine, Irvine, California 92697, USA.

[1] W. W. Heidbrink and G. J. Sadler, Nucl. Fusion **34**, 535 (1994).
[2] K. Toi *et al.*, Nucl. Fusion **40**, 1349 (2000).
[3] N. N. Gorelenkov, S. D. Pinches, and K. Toi, Nucl. Fusion **54**, 125001 (2014).
[4] L. Chen and F. Zonca, Rev. Mod. Phys. **88**, 015008 (2016).
[5] M. A. Van Zeeland *et al.*, Plasma Phys. Controlled Fusion **50**, 035009 (2008).
[6] M. A. Van Zeeland *et al.*, Nucl. Fusion **49**, 065003 (2009).
[7] M. A. Van Zeeland *et al.*, Nucl. Fusion **56**, 112007 (2016).
[8] A. Bortolon, W. W. Heidbrink, G. J. Kramer, J.-K. Park, E. D. Fredrickson, J. D. Lore, and M. Podestà, Phys. Rev. Lett. **110**, 265008 (2013).
[9] N. J. Fisch, Rev. Mod. Phys. **59**, 175 (1987).
[10] X. D. Du *et al.*, Phys. Rev. Lett. **114**, 155003 (2015).
[11] X. D. Du *et al.*, Nucl. Fusion **56**, 016002 (2016).
[12] N. B. Marushchenko, Y. Turkin, and H. Maassberg, Comput. Phys. Commun. **185**, 165 (2014).
[13] M. Osakabe *et al.*, Rev. Sci. Instrum. **72**, 590 (2001).
[14] S. Murakami *et al.*, Fusion Technol. **27**, 256 (1995).
[15] B. A. Carreras and P. H. Diamond, Phys. Fluids B **1**, 1011 (1989).
[16] H. L. Berk, B. N. Breizman, and H. Ye, Phys. Lett. **162A**, 475 (1992).
[17] G. Y. Fu and C. Z. Cheng, Phys. Fluids B **4**, 3722 (1992).
[18] B. N. Breizman and S. E. Sharapov, Plasma Phys. Controlled Fusion **37**, 1057 (1995).
[19] Ya. I. Kolesnichenko, V. V. Lutsenko, A. Weller, A. Werner, H. Wobig, Yu. V. Yakovenko, J. Geiger, and S. Zegenhagen, Nucl. Fusion **46**, 753 (2006).
[20] D. A. Spong, Phys. Plasmas **18**, 056109 (2011).
[21] H. Biglari and L. Chen, Phys. Fluids **29**, 2960 (1986).
[22] M. Isobe *et al.*, Rev. Sci. Instrum. **70**, 827 (1999).
[23] T. Nicolas and K. Ichiguchi, Nucl. Fusion **56**, 026008 (2016).
[24] K. Ichiguchi, J. Plasma Fusion Res. **3**, 576 (2000).
[25] L. Garcia, M. A. Ochando, A. Carreras, D. Carralero, C. Hidalgo, and B. Ph. van Milligen, Phys. Plasmas **23**, 062319 (2016).
[26] M. Wakatani, *Stellarator and Heliotron Devices* (Oxford University Press, New York, 1998).